Materials Science Forum
ISSN: 1662-9752, Vol. 1184, pp 97-112
doi:10.4028/p-5Z5Vcu

Submitted: 2026-01-19
Revised: 2026-02-23
Accepted: 2026-02-23
Online: 2026-04-14

Sliding Distance Dependency and Third Body Particle Influence in Flat Strip-Draw Testing of Aluminum Sheet for Friction Characterization in Automotive Stamping

Loris Rocchi[1,a*], Jan Filzek[2,b], Christian Leppin[1,c]

[1]Novelis R&D Centre Sierre, Switzerland

[2]FILZEK TRIBOtech, Mühltal, Germany

[a*]loris.rocchi@novelis.adityabirla.com, [b]filzek@tribotech.de,
[c]christian.leppin@novelis.adityabirla.com

Keywords: flat strip-draw test, automotive aluminum sheet, third-body particles, sliding distance.

Abstract. In automotive sheet metal stamping, the friction coefficient for a given tribological system (sheet, lubricant, tool surface) is known to depend on contact pressure, sliding velocity and temperature. Furthermore, plastic deformation of the sheet can cause surface roughening, which will affect frictional response. Beyond these known effects, the flat strip-draw experiments using friction pads of various sizes and repeated sliding on the same sample presented in this paper indicate that the frictional response depends on the sliding distance and sliding history. Moreover, we found that third body particles generated by the wear of sheet metal in frictional processes substantially influence the level of the friction force. Our results suggest that there is a need to improve the friction models implemented in current commercially available simulation software for aluminum sheet metal stamping, to capture these substantial effects.

Introduction

When determining the feasibility of a part in automotive sheet metal stamping, the elastoplastic deformation properties that define the formability of the sheet material are usually the focus. However, depending on the part and the die design, the frictional response can have just as much influence. Therefore, appropriate characterization and modeling of the tribological properties is important for the simulation-based forming process design of parts in the automotive industry [1]. Although it is still very common in the industry to use Coulomb friction [2], with a constant friction coefficient, it is well known that this assumption is incorrect, and that the actual friction between the sheet and the die in automotive stamping depends on local contact pressure [3], sliding velocity [4], lubrication [5],[6] and temperature [7], [8]. A further known effect is that for certain materials the plastic deformation of the sheet can cause surface roughening which will typically increase friction [9].

Flat strip-draw testing is a standard method for friction characterization in automotive applications. Beyond qualitative ranking of tribological systems, the test is used to identify friction-coefficient parameters for direct use in forming simulations and to calibrate multi-scale friction models [10], [11].

In aluminum stamping with uncoated cast-iron tools, a grayish transfer mark (Tribolayer) is often visible in regions of sliding contact, both on industrial parts and in laboratory strip-draw or drawbead tests. This transferred layer, commonly referred to as a tribolayer (third body particle, wear, and lubricant mix), forms under boundary lubrication from the interaction of the two contacting surfaces. The tribolayer coexists with topography evolution (surface flattening) that changes the real contact area [12]. In this paper, we demonstrate that the frictional response of aluminum sheets is influenced not only by changes in real contact area, but also by third body particles produced by wear. The relative contributions of these factors and their consequences for test-pad sizing in standardized strip-draw tests have not yet been systematically investigated.

Scope and contribution of this study to address these questions in three steps:
1) Implications for pad size and standards: We evaluate how the tribolayer's influence interacts with pad geometry, and we discuss consequences for pad-size selection in flat strip-draw testing.
2) Tribolayer composition: We characterize the chemistry and morphology of the tribolayer formed in aluminum-on-cast-iron contact under boundary lubrication.
3) Friction mechanism comparison: We quantify the tribolayer's contribution to the friction coefficient and compare it against the effect of surface flattening and the resulting real (as opposed to apparent) contact area. We further develop the observation to understand the tribolayer influence on the sliding distance and pressure history.
A practical motivation for step (3) is that VDA 230-213 [13] prescribes a pad size of 140 × 70 mm (length × width along the test direction). For typical automotive aluminum alloys, this rather large pad area limits the maximum attainable contact pressure in the test, which can be significantly lower than local pressures encountered in stamping die (e.g., in drawbeads) [14]. To bridge this gap, we complement the standard pad with smaller pads to access higher contact pressures and directly compare the resulting friction behavior to tests conducted at the VDA pad size.

Pad geometry Influence on Friction Results

Considerations for using different friction testing set-ups

During the flat strip draw friction test data acquisition, and as shown in Fig. 1, the following force sensor data is collected over time t: the normal force $F_N(t)$, and the frictional response forces $F_{T1}(t)$ and $F_{T2}(t)$ of each individual friction pad, and the pulling force $F_p(t)$ at the grip of the sample. With $F_P(t) = F_{T1}(t) + F_{T2}(t)$, and the nominal contact surface of each pad A, the nominal average frictional shear stress acting on the pads can be defined as:

$$T(t) = \frac{F_P(t)}{2\,A} \tag{1}$$

and the nominal contact pressure as:

$$p(t) = \frac{F_N(t)}{A} \tag{2}$$

The instantaneous average friction coefficient over time is then given by:

$$\mu(t) = \frac{\tau(t)}{p(t)} = \frac{F_P(t)}{2\,F_N(t)} \tag{3}$$

VDA 230-213 defines the size of the friction pad $A = l\,x\,w = 140\ mm\ x\ 70\ mm$ (pad length in testing direction l, pad width w). Depending on the strength and thickness of the tested material sheet, as well as the resulting friction coefficient, the rather large pad length defined by the standard limits the normal force, respectively the normal contact pressure to values which are between 10 to 20 MPa for typical automotive aluminum sheet. However, the highest values observed locally in real automotive sheet metal stamping processes can be in the range of 50 MPa and even higher. At least, this is what numerical stamping process simulations suggest, since measuring local contact pressure in real dies directly is difficult [14]. Our original motivation for using smaller friction pad sizes was to overcome this issue and achieve higher nominal contact pressures in the test.

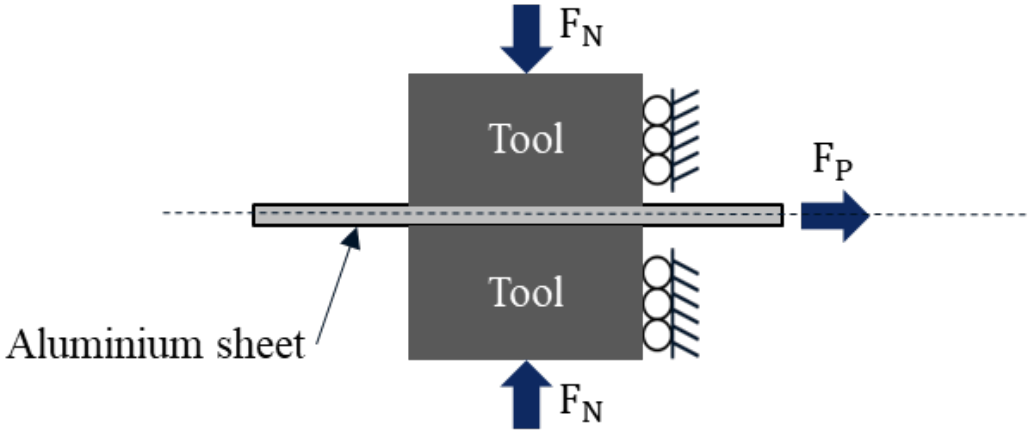

Fig. 1. Schematic of standard single test sample configuration (si) for flat strip-draw testing.

As a further method to achieve higher nominal contact pressures we applied an innovative sandwich sample testing method. Instead of only one sheet sample, this method uses two samples lubricated only on the side which is in contact with the friction pads of the test equipment, and with a steel sample at the core between the two test samples, see scheme shown in Fig. 2. With the dry side of each test sample contacting the steel core, this sandwich sample testing configuration is designed to avoid any relative movement between the aluminum test samples and the steel core, which was verified by measuring before and after the sample length. It therefore prevents elongation and thinning of the test samples. Consequently, the friction coefficient can be measured independently of sample elongation, which is often observed at higher nominal contact pressure levels using the single sample method, and which may induce surface roughening that can considerably influence the frictional response. In general, none of the tests presented in this paper showed galling, meaning there was no visual adhesion of aluminum to the tool.

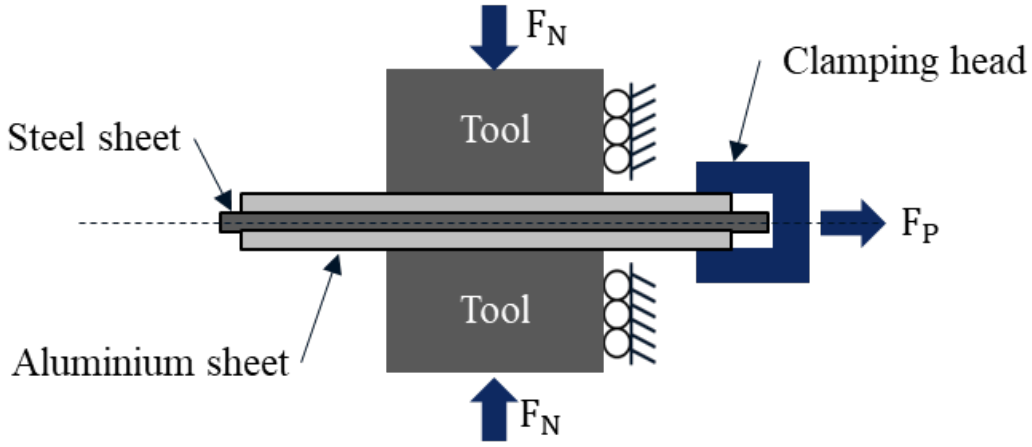

Fig. 2. Schematic of sandwich test sample configuration (sw) for flat strip-draw testing.

Friction pads and test sample sizes used in the friction tests

The friction pads are made of EN-GJS-700-2 cast iron. Each friction pad's surface is machined by rotary grinding to the surface roughness $S_a = 0.3$ µm. Table 1 provides an overview of the friction pad sizes (testing direction l times width w effective contact area without the transition radius) and the corresponding test sample sizes used in the friction tests. Specimen width exceeds pad width to minimize edge effects and ensure the central contact zone experiences uniform nominal pressure.

Table 1. Friction pad sizes (contact area) and test sample sizes used in the friction tests.

Pad size (l × w)	Test sample size (l × w)
35 mm × 35 mm	600 mm × 50 mm
70 mm × 35 mm	600 mm × 50 mm
140 mm × 35 mm	600 mm × 50 mm
140 mm × 70 mm	600 mm × 100 mm

Sheet materials and friction test conditions

Three different aluminum sheet variants were tested, see also Table 2: An aluminum alloy AA 6014 T4 with an EDT surface, as well as the same alloy with a mill finish surface (MF). Additionally, an aluminum alloy AA 5182-O with an EDT surface was tested. The sheet thickness for all variants was 1.0 mm. The test specimens were lubricated with $0.8\,g/m^2$ of Walter Zepf Al200 using electro discharge equipment to ensure homogeneous application of the lubricant. The friction tests presented in this section were performed in rolling direction (later denoted by L), at a temperature of 40 °C, and at a constant sliding speed of 80 mm/s.

Table 2. Tested sheet material variants.

ID	Material	
21	AA 6014-T4	EDT
22	AA 6014-T4	MF
23	AA 5182-O	EDT

Results of friction tests with different pad geometries and discussion

All of the friction coefficients presented here as a function of nominal contact pressure are values based on steady-state testing conditions after the initial static peak of each test. Fig. 3 shows the results for the flat strip-draw tests using different friction pad sizes with the sheet material variant AA 6014-T4 EDT. Even though the tribological system and testing conditions are the same for each curve, the test results are heavily influenced by the friction tool geometry. Fig. 4 shows the nominal average frictional shear stress as a function of nominal contact pressure, which is the same data, but without division by the nominal contact pressure. At low contact pressure, the shear stresses are nearly identical and approach zero. As pressure increases, the gap between some curves grows while others show the same trend. For example, at 30 MPa, both the 140x70 mm² and the 140x35 mm² pads show a shear stress of approximately 0.6 MPa despite their twofold width difference. However, at the same pressure, the shear stresses reported for the 70x35 mm² and 35x35 mm² pads are 1 and 1.8 MPa, respectively. These values are almost double and triple those for pads of the same width but different lengths. Therefore, the test results at the same pressure show a strong dependency on friction pad length. In contrast, pads of the same length but different widths show only marginal differences when considering the measurement uncertainty of the test. Examining the friction coefficient representation of the results more closely, one might argue that the tests using a 140 mm x 35 mm pad differ from the tests using the same length with twice the width (70mm) at low contact pressures (single sample and sandwich sample). However, we believe that this difference is due to the considerably increased measurement uncertainty at low contact pressures. In the frictional shear stress representation of the same results, this difference is considerably less pronounced and the overall trend of the dependency on pad length dominates is confirmed. Moreover, no significant difference was observed between the standard single test sample configuration (si) and the sandwich test sample configuration (sw), which indicates that elongation and thinning doesn't play a significant role in the cases which have been tested in standard single sample configuration.
The test results for the variants AA 6014-T4 MF shown in Fig.6 and AA 5182-O EDT shown in Fig.5 confirm the observations discussed above.

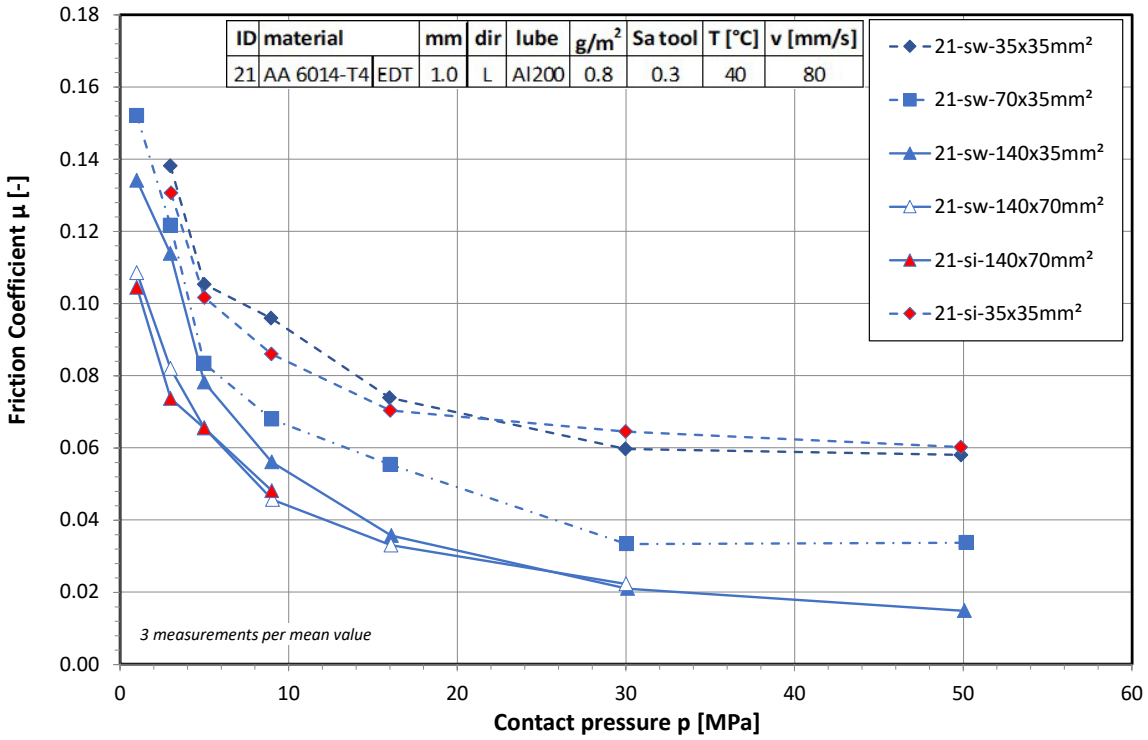

Fig. 3. Friction coefficient as a function of nominal contact pressure from flat strip-draw friction test results with AA 6014-T4 EDT (ID 21) with identical tribological system for different sized friction pads (length in sliding direction x width). Tests were performed using either a standard single test sample test configuration (si) or a sandwich test sample configuration (sw). Aside from different nominal contact pressures, test conditions are identical.

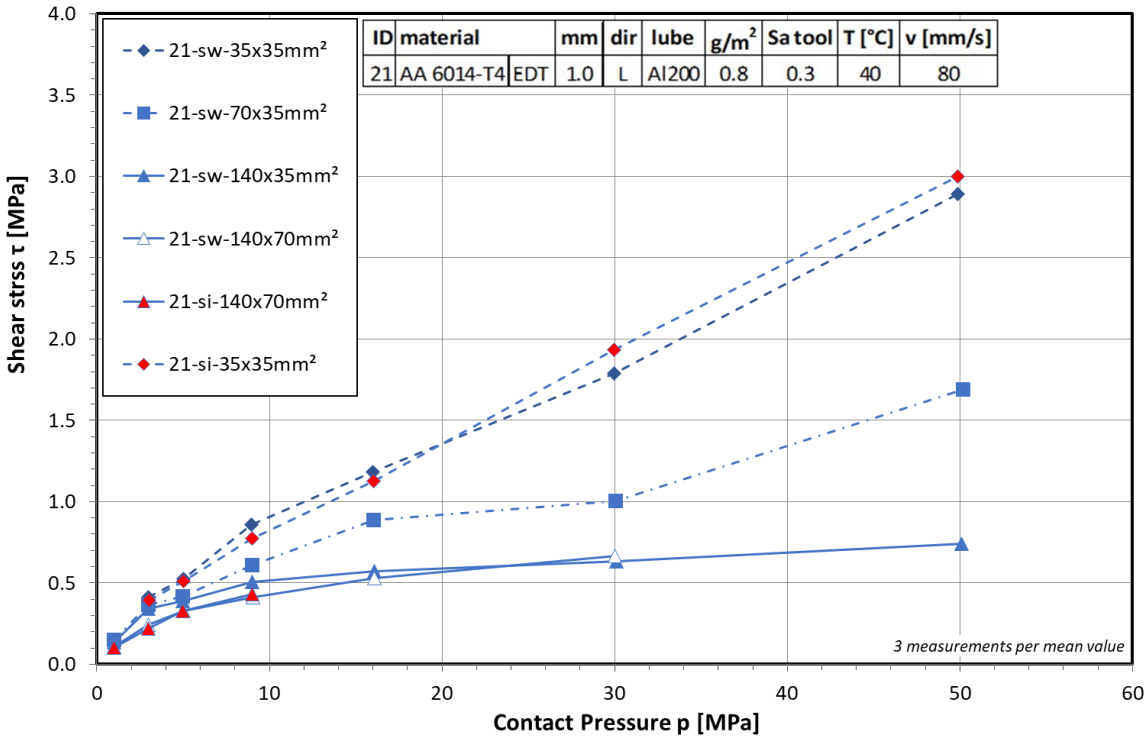

Fig. 4. Frictional shear stress as a function of nominal contact pressure from flat strip-draw friction test results with AA 6014-T4 EDT (ID 21) with identical tribological system for different sized friction pads (length in sliding direction x width). Tests were performed using either a standard single test sample test configuration (si) or a sandwich test sample configuration (sw). Aside from different nominal contact pressures, test conditions are identical.

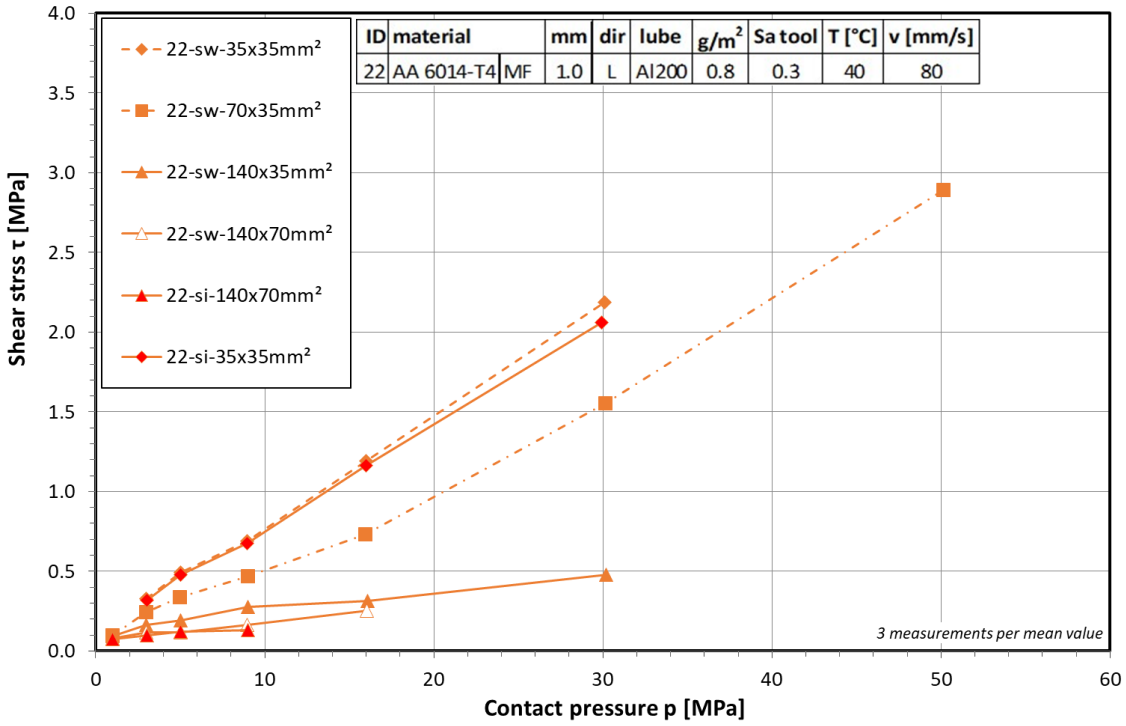

Fig. 5. Frictional shear stress as a function of nominal contact pressure from flat strip-draw friction test results with AA 6014-T4 MF (ID 22) with identical tribological system for different sized friction pads (length in sliding direction x width). Tests were performed using either a standard single test sample test configuration (si) or a sandwich test sample configuration (sw). Aside from different nominal contact pressures, test conditions are identical.

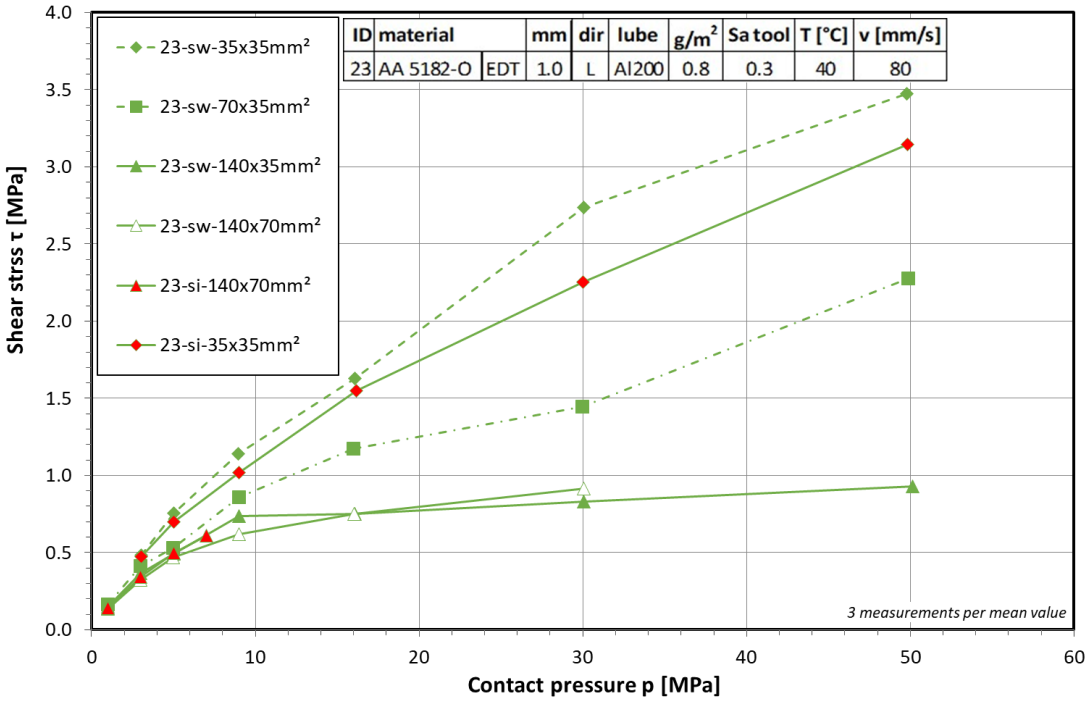

Fig. 6. Frictional shear stress as a function of nominal contact pressure from flat strip-draw friction test results with AA 5182-O EDT (ID 23) with identical tribological system for different sized friction pads (length in sliding direction x width). Tests were performed using either a standard single test sample test configuration (si) or a sandwich test sample configuration (sw). Aside from different nominal contact pressures, test conditions are identical.

Analysis of the Tribo-Layer and Abrasion

This section describes the analysis of the surface texture evolution, as well as the investigation of the grayish mark that develops along the sliding track of a flat strip-draw sample (Fig.8), and which also can be observed on stamped parts (Fig. 7).

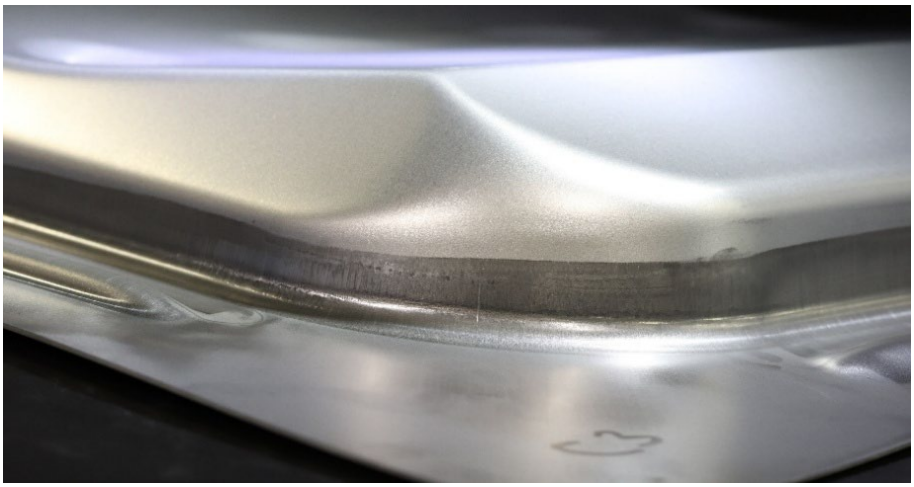

Fig. 7. Deep drawn stamping part showing typical grayish tribolayer in areas which experienced increased contact pressure.

Fig. 8. Sliding tracks on flat strip-draw friction test samples are visible as a grayish mark.

Methods for third body debris characterization and analyzing surface texture evolution

To characterize the constituents of the third-body (tribolayer) associated with the frictional contact, debris was collected from test samples by rinsing the sliding track with toluene and filtering the rinse. The collected material was weighed and examined by scanning electron microscopy (SEM) to assess the morphology of the observed particles. Additionally, laser diffraction was employed to determine the particle-size distribution.

To quantify changes in surface texture caused by frictional sliding, the test specimens of the flat strip-draw test results presented in the previous section were first marked with a microhardness indentation as of approximately 100 µm (fiducial marker) to enable precise localization of the same region before and after testing. Then, confocal laser scanning microscopy (CLSM) was performed on both the aluminum sheets and the tool pads in regions outside the specimen edges. Prior to lubrication and friction testing, each marked location was imaged at 20× magnification over a 2×2 mm² area. The area was scanned with 3432×3432 points (lateral spacing 0.67 µm) to obtain a high-resolution, three-dimensional height map. After imaging, the specimens were lubricated and tested in a flat strip-draw. After testing, the surfaces were rinsed with toluene and were re-imaged at the identical location by returning to the reference indentation to ensure spatially consistent before-and-after comparisons.

Tribolayer analysis and composition

Fig. 9 shows the weight per area of the filtered and converted particles from the cleaning rinse collected from friction test samples of material 23 of the corresponding test series in the previous section. As can be seen, the recovered particulate mass increases with the contact pressure applied in the friction test. This trend is plausible, as higher contact pressure will result in greater indentation by the tool, which likely abrades and mobilizes more third-body debris from the surface.

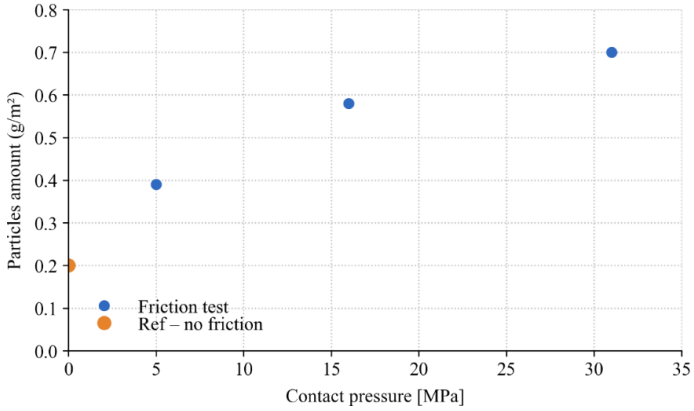

Fig. 9. Weight per area of filtered and converted particles depending on contact pressure.

The SEM image in Fig. 10 shows flake-like debris of material 23 tested at 5MPa contact pressure. The lateral dimensions of the debris particles are markedly larger than the thickness. To evaluate the composition of the tribolayer and adhering particles, energy-dispersive X-ray spectroscopy (EDS) was performed at three locations across the surface. The elemental results are summarized in Table 2. The detected carbon is attributed to the conductive carbon tape used as the mounting support. The analysis indicates that the particles are composed predominantly of aluminum and aluminum oxide. The percentage weight values indicate that the particles are aluminum-rich, with Al contents between 55.58 and 82.06 wt% and measurable oxygen (1.30–20.26 wt%), consistent with the presence of alumina within the tribolayer. Some magnesium is detected (2.14–2.74 wt%), while titanium and manganese appear only at trace levels (≤ 0.22 wt% each); silicon and iron were not detected. The carbon signal (13.63–24.72 wt%) is attributed to the conductive carbon tape used for mounting and does not represent the intrinsic particle composition.

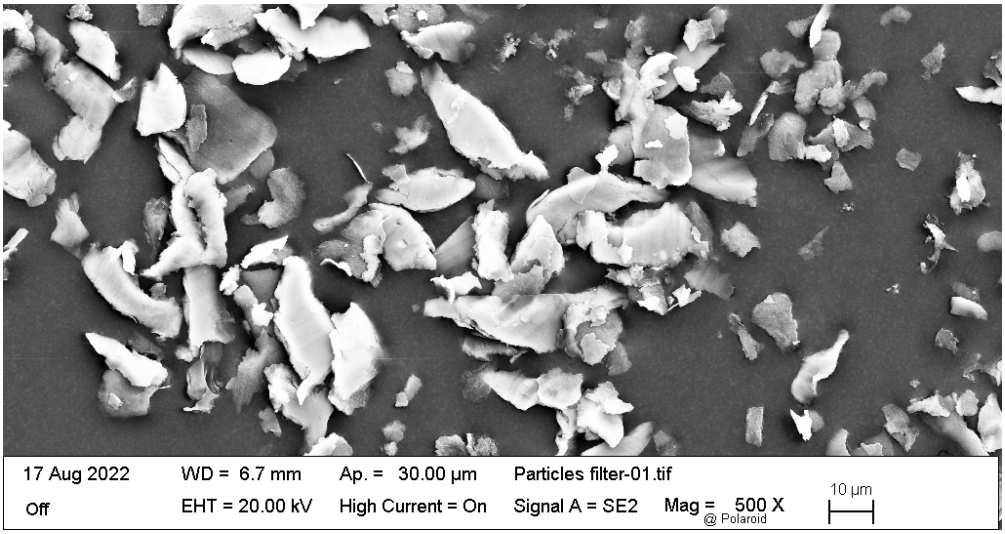

Fig. 10. SEM image of wear debris generated during a flat strip-draw friction test.

Table 3. EDS measurement of the collected wear debris.

Spectrum Label	C [wt%]	O [wt%]	Mg [wt%]	Al [wt%]	Si [wt%]	Ti [wt%]	Mn [wt%]	Fe [wt%]
Spectrum 1	13.63	1.3	2.74	82.06	0	0.05	0.22	0
Spectrum 2	19.68	20.26	2.48	57.27	0	0.19	0.13	0
Spectrum 3	24.72	17.13	2.14	55.58	0	0.22	0.21	0

Particles size

Particle-size distributions were obtained using a Mastersizer 3000 (Malvern Panalytical) operated in wet dispersion with toluene as the suspending medium. Laser diffraction yields volume-weighted, sphere-equivalent diameters. For thin flake-like debris, these diameters predominantly reflect the in-plane extent rather than the out-of-plane thickness. Accordingly, the distribution shown in Fig. 11 should be interpreted in conjunction with the SEM image Fig. 10, which confirms a flake morphology with submicron thickness.

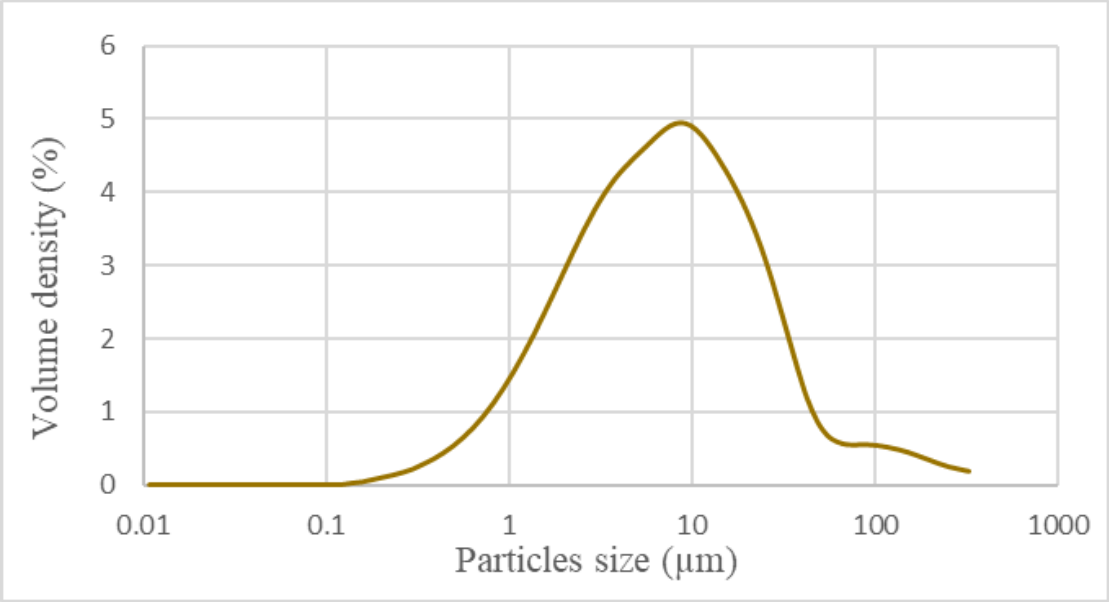

Fig. 11. Particles size distribution associated with the material tested with the Std 70x140mm^2 pads.

Quantification of surface topography change by before-and-after observation

We quantified the evolution of surface topography on the aluminum sheet by comparing confocal scans acquired before and after friction testing at the same location. The two height maps were registered using a feature-based algorithm developed by Colin Majoor [15] that uses the EDT or MF valleys as fiducials to align the before and scan results. See Fig. 12 as an example of such an analysis, where image (d) presents the difference map, $\Delta z = z_{before} - z_{after}$, which reveals topographic changes at the pixel level: $\Delta z > 0$ denotes local material removal (abrasion or asperity flattening), and $\Delta z < 0$ indicates local uplift, respectively pile-up due to plastic flow. This approach provides a spatially resolved visualization of abrasion.

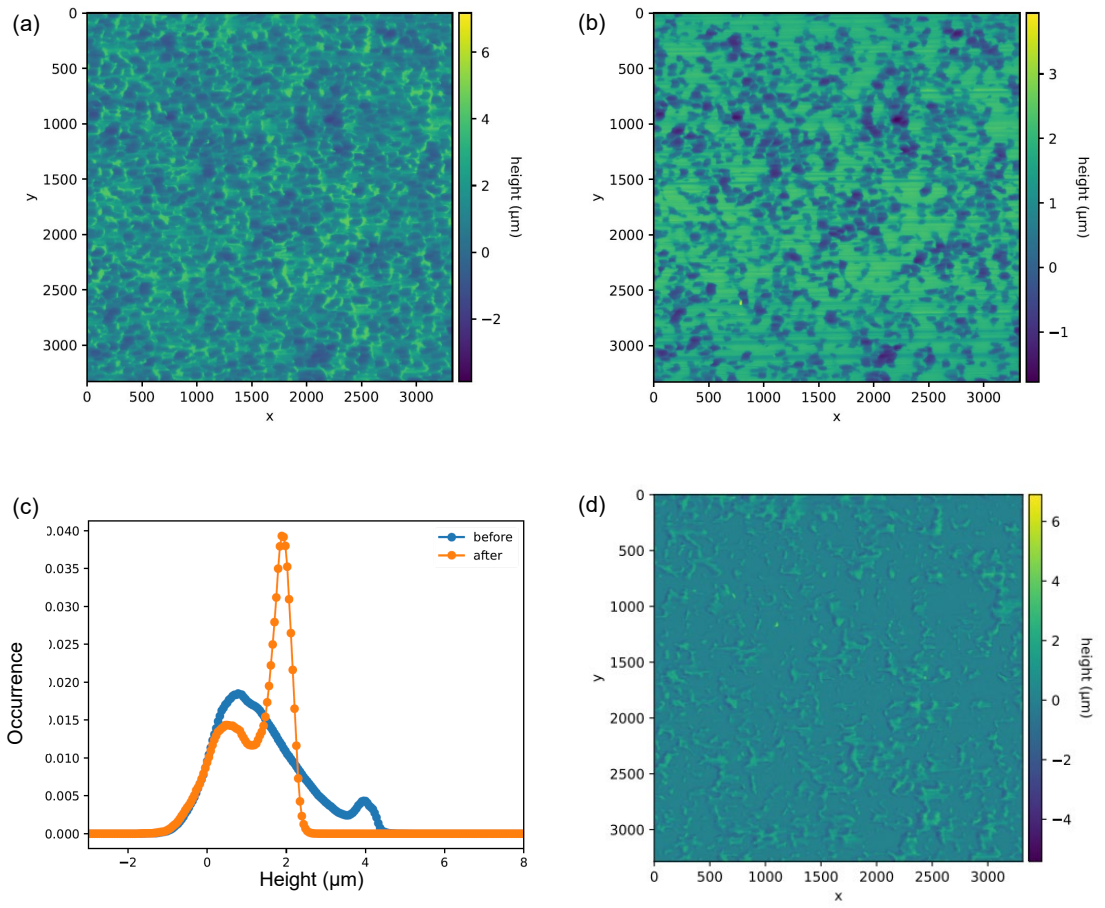

Fig. 12. Before-and-after analysis of the surface of material 21 tested at 9 MPa: (a) Color map of the confocal observation before friction test; (b) Color map of the confocal observation after friction test; (c) Height distribution of images (a) and (b); (d) Color map image of the subtraction of the confocal image after (b) from the confocal image before friction test (a).

Influence of Abrasion and Tribolayer in Multiple Draws

Building on the investigation of the pad geometry influence in the initial section of this paper and the analysis of the tribolayer in previous section, this section examines how the surface flattening, abrasion and the tribolayer formation during sliding affect the friction coefficient. We attempt to evaluate the contribution of each of these mechanisms. For this purpose, we designed various flat strip-draw testing sequences in which the same sample is drawn multiple times on the same sliding track, as schematically shown in Figure 13.

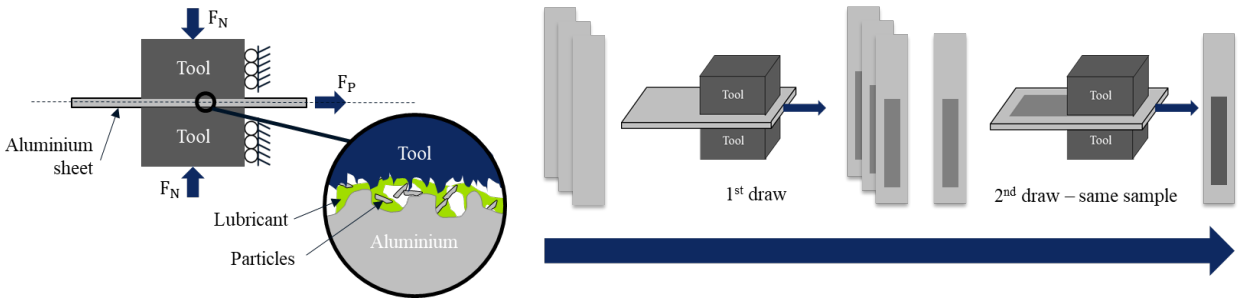

Fig. 13. Sequence of multiple draws of the same samples on the same sliding track to investigate the influence of surface flattening, abrasion and tribolayer creation.

Unless explicitly mentioned otherwise, the following constituents are used in all tests presented in this section: Aluminum alloy AA 5182, 1.5 mm thickness with an EDT surface. The test specimens were lubricated with Walter Zepf Al200 with $1.0\ g/m^2$ using electro discharge equipment. Cast iron EN-GJS-700-2 friction pads with a milled 35 mm × 35 mm contact surface and S_a in the range 0.20–0.25 μm were used.

Experiments to single out the effect of the tribolayer

The following three different experimental sequences involving multiple draws on the same sample were performed:

- Experimental sequence A: The sample is drawn twice at 6 MPa contact pressure on the same sliding track (sample is drawn as is after the first draw, therefore the tribolayer is preserved).
- Experimental sequence B: The sample is drawn twice at 6MPa contact pressure on the same sliding track, with cleaning using MEK and re-lubrication with original amount before the 2nd draw (the tribolayer is removed).
- Experimental sequence C: The sample is drawn four times at 10 MPa contact pressure on the same track, with cleaning using MEK and re-lubrication with original amount before the 4th draw (the tribolayer is preserved before the 2nd and 3rd draw, but it is removed before the 4th draw).

In all three sequences the following test conditions were applied: testing in rolling direction at a room temperature (RT) and a sliding speed of 5 mm/s.

Fig. 14 shows that, in experimental sequence A, testing at 6 MPa, the second draw reduces the friction coefficient by 44% from 0.161 to 0.093. Conversely, experimental sequence B, also testing at 6 MPa, but the second draw occurring after cleaning and re-lubrication, the friction coefficient decreases considerably less from 0.160 to 0.151. Sequences A and B result in the same flattened sheet surface texture after the first draw and we assume the same real contact area results of those two tests at the start of the second draw. However, in sequence B the particle-rich tribolayer is removed, and the sample is freshly lubricated, potentially with even slightly more lubricant than the sample in sequence A after the first draw, as some lubricant may have been displaced from the sliding track. This result suggests that the tribolayer exerts a far stronger influence on friction in aluminum than the surface texture flattening alone and the resulting change of real contact surface area.

Furthermore, Fig. 14 shows that in experimental sequence C (testing at 10 MPa), the friction coefficient decreases from 0.127 to 0.07 to 0.055 in the second and third draws, where the developed tribolayer is preserved. However, after cleaning the sample with MEK and re-lubricating it to the original amount prior to the fourth draw, the friction coefficient increases almost to the level of the first draw (approximately 0.12). This provides further strong evidence of the tribolayer's dominant influence on friction in aluminum shown in experimental sequence C.

Our interpretation of the observed behavior is that the flake-like debris in combination with the lubricant forms a tribolayer that acts as a separator between the tool and the aluminum surface, thereby reducing plowing of the tool into the flattened surface asperities. Preserving the tribolayer considerably reduces the shear resistance of this interface, causing the pronounced drop in friction coefficient shown in Fig. 14.

Finally, we would like to point out that all three sequences were performed without any galling being visually observed between any of the draw repetitions.

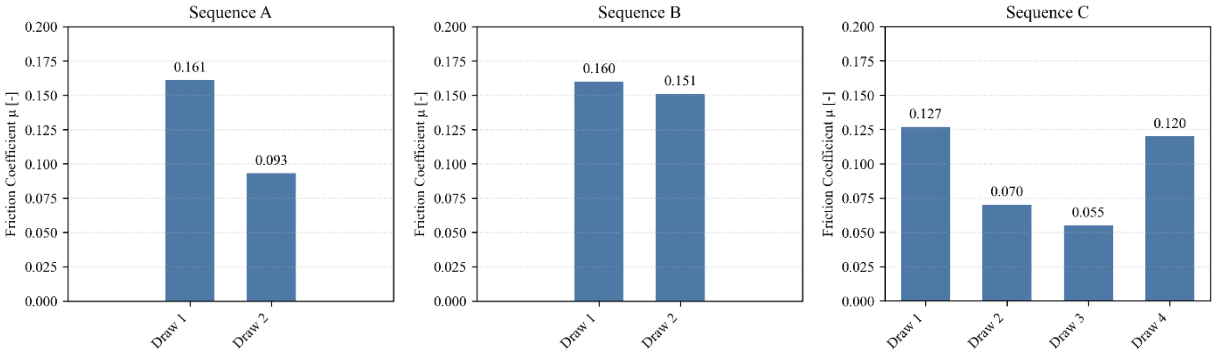

Fig. 14. Effect of tribolayer on the evolution of the friction coefficient in flat strip-draw friction tests with multiple drawing of the same sample: experimental sequence A: sample used as is in 2nd draw, experimental sequence B: sample cleaning and re-lubrication before 2nd draw, experimental sequence C: sample used as is in 2nd and 3rd draw, cleaning and re-lubrication before 4th draw.

Friction tests with multiple draws on the same sample

The following two different experimental sequences involving multiple draws on the same sample were performed:

- Experimental sequence D: Each sample is repeatedly drawn at the same contact pressure as in the first draw (3 draws for each sample in total).
- Experimental sequence E: Each sample is drawn with 7 MPa nominal contact pressure in the 1st draw. Various contact pressures are applied in the 2nd draw of a sample.

In both sequences the following test conditions were applied: testing in rolling direction at a room temperature (RT) and a sliding speed of 5 mm/s.

The results in Fig. 15 show that in experimental sequence D, where the same contact pressure is repeatedly applied to each sample, the friction coefficient decreases with each draw. Based on the observations in experimental sequences A, B and C, we assume this reduction is mainly caused by the tribolayer rather than the surface flattening. For most contact pressures, the decrease in the friction coefficient between the first and the second draw is greater than the decrease between the second and the third draw, except in the test sequence at the lowest contact pressure of 2 MPa. In experimental sequence E, each sample is first tested at a contact pressure of 7 MPa creating the same amount of wear in the tribolayer. Then samples are tested at different contact pressures in the second draw, and the following can be observed: the smaller the contact pressure in the second draw compared to the initial 7 MPa draw, the greater the decrease in the friction coefficient. Conversely, the greater the contact pressure in the second draw compared to the initial 7 MPa draw, the smaller the decrease in the friction coefficient. In the latter case, the friction coefficient results of the second draw converge to those of the first draw at the same contact pressure in sequence D. With increasing contact pressure, the initial 7 MPa draw in sequence E has a vanishing effect.

The curve of the second draw shows the opposite trend after testing all samples at 7 MPa, considering that the friction coefficient curves typically decrease monotonically with increasing contact pressure. However, in anticipation of expected changes to the surface texture and particle formation in the preliminary test at 7 MPa, it is plausible that, in subsequent draws at lower contact pressures, the reduction in the coefficient of friction is more significant while, at higher contact pressures, the reduction is less significant. In any case, this experiment demonstrates that the contact pressure history should be considered when modeling and characterizing the frictional response of aluminum sheets.

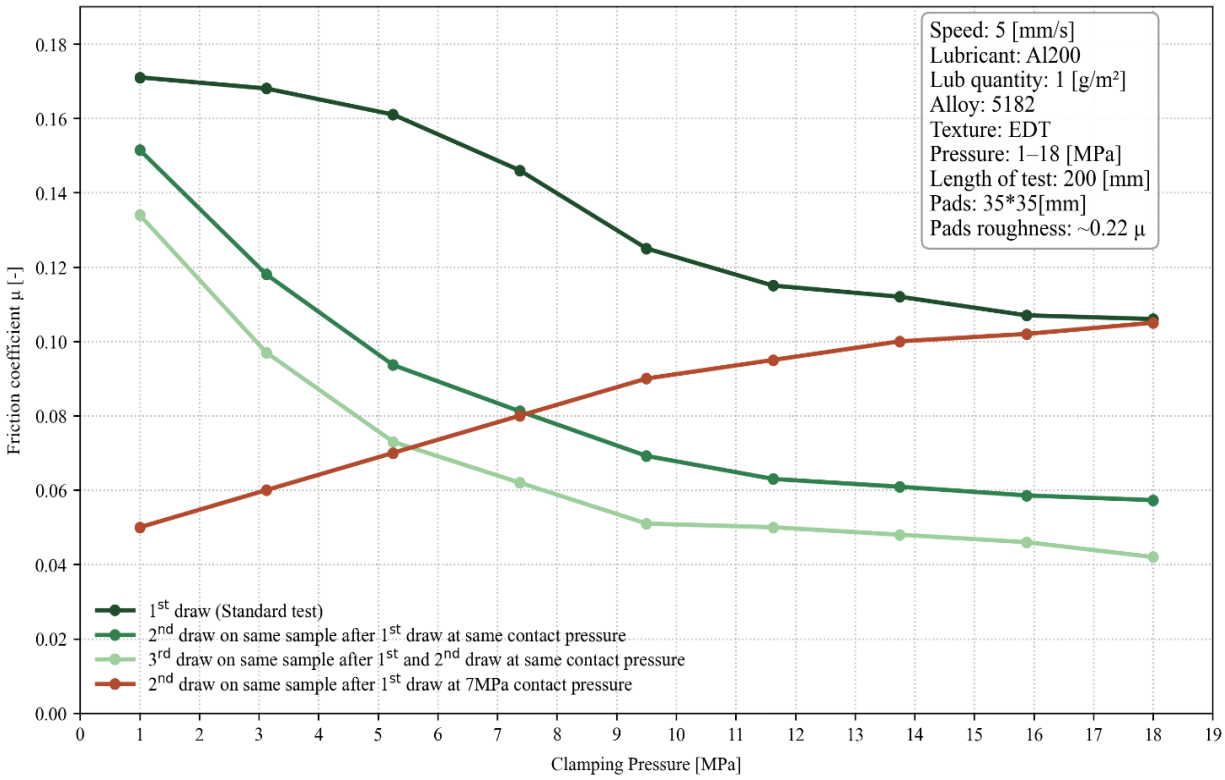

Fig. 15. Friction tests with AA 5182-O EDT and lubricant Al200 – Development of the friction coefficient in friction tests with multiple draws on the same sample. Results for sequence D (each sample repeatedly drawn at same contact pressure as in 1st draw, 3 draws in total), and results for sequence E (1st draw at 7 MPa, 2nd draw at different contact pressures).

Comparison of long pad results with multiple draw tests using short pads

The first of two experimental sequences in this subsection follows sequence D and adds a fourth draw of each sample on the same sliding track at the same contact pressure. Tests were performed again in rolling direction, but at a temperature of 40°C instead of RT, and at a considerably higher sliding speed of 100 mm/s. The second sequence in this subsection is almost identical, except that only the first draw is applied to each sample, and that four times longer friction pads are used (testing direction l x width w = 140mm x 35mm). Fig. 16 shows the friction coefficient results for the single draw of the test series using the standard 140 mm x 35 mm friction pads, as well as the results for each draw of the experimental sequence using 35 mm x 35 mm friction pads, which are four times shorter. Consistent with the results presented in the initial section of this paper investigating the influence of pad geometries, the friction coefficient curve for the first draw with the shorter friction pads is significantly higher than that for the 4x longer friction pads. Furthermore, as in the previously presented experimental sequence D with three draws, the friction coefficient curve for the shorter pads drops with every additional draw in decreasing step sizes. The friction coefficient curve resulting from averaging the curves from the four draws with the short pads corresponds well to the curve from the long pads. This allows the conclusion that the test with 4x longer pads corresponds to a test with a train of four coupled short pads where the friction coefficient contact zone decreases in sliding direction (highest friction coefficient at pad entry point, lowest friction coefficient at pad exit point).

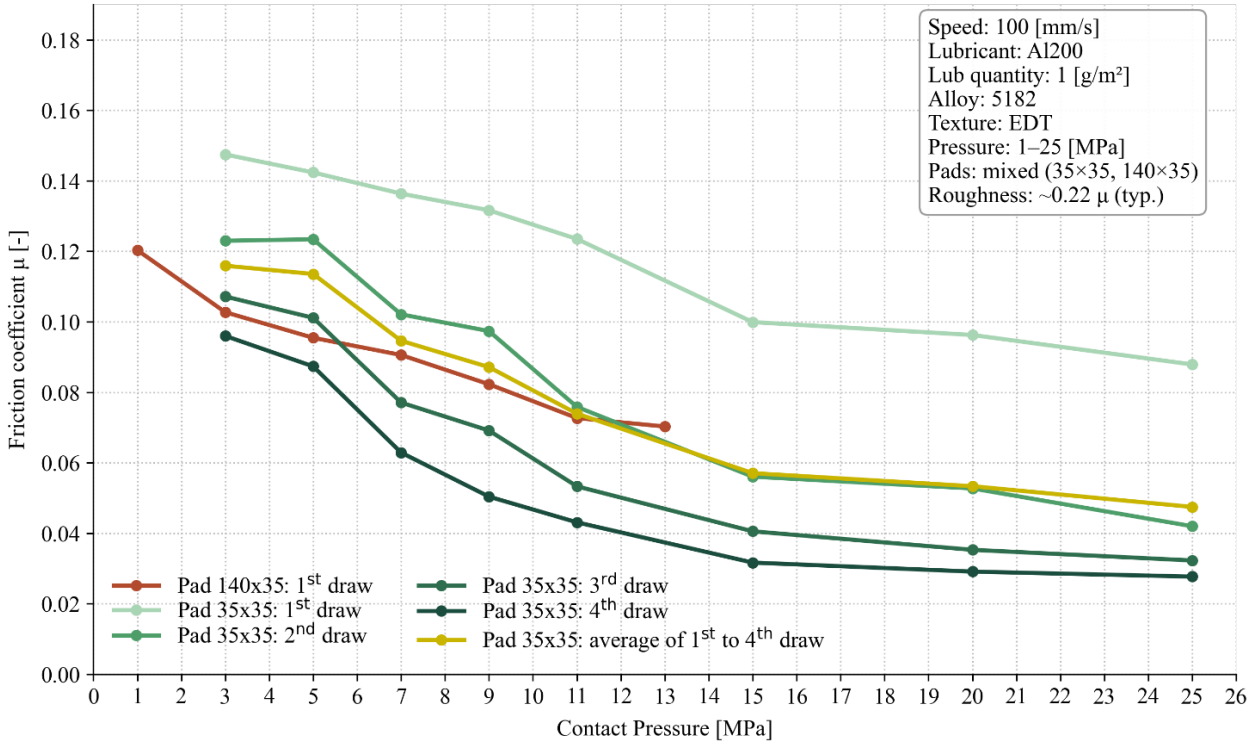

Fig. 16. Friction tests with AA 5182-O EDT and lubricant Al200 – Friction coefficient results for standard test series using long friction pads (only 1st draw) and test series with multiple draws using 4 times shorter friction pads (4 draws in total).

Conclusion

For boundary-lubricated automotive aluminum sheet, this paper demonstrates in detail the following points:

1. The geometry of the pads is a key factor in determining the friction coefficient. Pads of the same length but different widths produce a comparable friction coefficient. However, changing the length produces completely different results.
2. Third body particle mass collected increases with pressure. The particles are flake-like consisting predominantly of aluminum and aluminum oxide. Confocal microscopy can be used to quantify the amount of abrasion and the flattening of the surface texture.
3. The tribolayer induces a stronger reduction of friction coefficient than surface flattening and real area of contact. Cleaning and relubrication results in modest changes to the friction coefficient, which remains close to the initial value. Whereas, preserving the tribolayer results in reductions.
4. The sliding history is of great importance. When the test is repeated with the tribolayer preserved, the friction coefficient can decrease by up to 40–50%. Altering the sliding history so that the initial draw is at 7 MPa rather than at the same pressure results in the opposite trend of a standard pressure-dependent friction curve.
5. The friction coefficient can be normalized by the cumulative sliding length. Four passes with a 35 × 35 mm^2 friction pad are equivalent to a single pass with a 140 × 35 mm^2 pad (considering measurement uncertainty). It supports the use of effective sliding distance approach.

These points and their implications raise discussion points for characterization and simulation: (i) Flat strip-draw tests show that, for automotive aluminum, the measured friction coefficient varies with pad length. Therefore, caution should be exercised when using such measurements directly to determine friction parameters in modeling. (ii) These results and our additional tests involving multiple draws on the same sample at different pressures reveal that the frictional response depends

on the contact pressure history. (iii) From an applied-mechanics standpoint, the friction coefficient of a material point decreases along the contact path from entry to exit. We assume that a homogeneous friction coefficient across the pad is invalid for aluminum, and that the friction coefficient must be treated as a function of sliding distance.

Acknowledgement

A significant portion of the results presented in this paper were obtained in connection with the InnoSuisse project 100.777 IP-ENG funded by the Swiss Federal Government in collaboration with the Computational Solid Mechanics Laboratory at the Ecole Polytechnique Fédérale de Lausanne, EPFL, Switzerland, under the direction of Prof. Jean-François Molinari. We thank Prof. Jean-François Molinari and his team members Dr. Guillaume Anciaux, Dr. Parissa Alavi, and MSc. Colin Majoor for the very productive technical discussions and constructive feedback on the experimental work, data analysis, and interpretation. In particular, we would like to express our gratitude for the opportunity to present results of Colin Majoor's master's thesis in this publication [15]. Any errors remaining in this publication are the responsibility of the authors. The authors are solely responsible for the content, which does not reflect the views of EPFL or the InnoSuisse organization.

References

[1] M. Sigvant et al., Friction in sheet metal forming: influence of surface roughness and strain rate on sheet metal forming simulation results, Procedia Manuf., vol. 29, 2019, DOI 10.1016/j.promfg.2019.02.169.

[2] C.-A. de Coulomb. “Essai sur une application des règles de maximis et minimis à quelques problèmes de statique, relatifs à l’architecture”. In: Mémoires de Mathématique et de Physique, présentés à l’Académie Royale des Sciences 7 (1776).

[3] J. Filzek, M. Ludwig, and P. Groche, Improved FEM simulation of sheet metal forming with friction modelling using laboratory tests, Proc. IDDRG, Bilbao, Spain, pp. 5–8, 2011.

[4] K. J. Lee and M. G. Lee, Pressure and sliding velocity dependent surface asperity based friction model: Application to springback simulation, IOP Conf. Ser. Mater. Sci. Eng., vol. 651, Nov. 2019, DOI 10.1088/1757-899X/651/1/012079.

[5] M. Sigvant et al., Friction in Sheet Metal Forming Simulations: Modelling of New Sheet Metal Coatings and Lubricants, IOP Conf. Ser. Mater. Sci. Eng., vol. 418, Sep. 2018, DOI 10.1088/1757-899X/418/1/012093.

[6] P. Alavi, G. Anciaux, L. Rocchi, J. Richard, J.F. Molinari. Numerical modeling of rough contact interfaces with trapped compressive liquid pockets. Tribology International. Volume 214, Part A, 2026, 111142. DOI:10.1016/j.triboint.2025.111142.[doi.org].

[7] D. Waanders, J. H. Marangalou, M. Kott, S. Gastebois, and J. Hol, Temperature Dependent Friction Modelling: The Influence of Temperature on Product Quality, Procedia Manuf., vol. 47, 2020, DOI 10.1016/j.promfg.2020.04.159.

[8] Filzek, J., Keil, D., & Schröder, H. (2021). Temperature induced friction increase in friction test and forming demonstrator for sheet metal forming. ESAFORM 2021 Proceedings. DOI: 10.25518/esaform21.3732.

[9] F. Jalali Moghadas, M. de Rooij, T. van den Boogaard, J. Hazrati, Effect of Normal Load and Bulk Strain on Real Area of Contact in Aluminum Sheet Forming.

[10] J. Hol. “Multi-scale friction modeling for sheet metal forming”. PhD thesis. Enschede, The Netherlands: University of Twente, 2013.

[11] P. Alavi, G. Anciaux, J.F. Molinari, L. Rocchi, C. Leppin. A multiscale model of friction considering the influence of third-body wear particles. arXiv, 2510.13470. DOI: 10.48550/arXiv.2510.13470 [doi.org].

[12] Bowden, F.P. & Tabor, D. The Friction and Lubrication of Solids. Oxford University Press, reprint ed. 2001.

[13] VDA 230-213 (2022). Testing procedure for product classes Prelube, Prelube 2, Hotmelt, Spot lubricant. Verband der Automobilindustrie e.V. (VDA).

[14] J. Cillaurren, L. Galdos, Ma. Sanchez, A. Zabala, E. Saenz de Argandoña J. Mendiguren. Contact pressure and sliding velocity ranges in sheet metal forming simulations.

[15] C. Majoor, Image correlation and data analysis applied to surface texture microscopy, master thesis, Ecole Polytechnique Fédérale Lausanne, 2023.